This Accepted Manuscript has not been copyedited and formatted. The final version may differ from this version.

eNeuro

Research Article: Methods/New Tools | Novel Tools and Methods

In vivo two-photon imaging of dendritic spines in marmoset neocortex

Two-photon imaging of spines in marmoset cortex

Osamu Sadakane[1,2], Akiya Watakabe[1,2], Masanari Ohtsuka[1,2], Masafumi Takaji[1,2], Tetsuya Sasaki[3], Masatoshi Kasai[4], Tadashi Isa[4], Go Kato[5], Junichi Nabekura[5], Hiroaki Mizukami[6], Keiya Ozawa[6], Hiroshi Kawasaki[7] and Tetsuo Yamamori[1,2]

[1]Laboratory for Molecular Analysis of Higher Brain Function, Brain Science Institute, RIKEN, Wako, Saitama 351-0198, Japan

[2]Division of Brain Biology, National Institute for Basic Biology, Aichi 444-8585, Japan

[3]Department of Ultrastructural Research, National Center of Neurology and Psychiatry, National Institute of Neuroscience, Tokyo 187-8502, Japan

[4]Division of Behavioral Development, National Institute for Physiological Science, Aichi 444-8585, Japan

[5]Division of Homeostatic Development, National Institute for Physiological Science, Aichi 444-8585, Japan

[6]Division of Genetic Therapeutics, Center for Molecular Medicine, Jichi Medical University, Tochigi 329-0498, Japan

[7]Department of Biophysical Genetics, Graduate School of Medical Sciences, Kanazawa University, Ishikawa 920-8640, Japan

DOI: 10.1523/ENEURO.0019-15.2015

Received: 27 February 2015

Revised: 3 July 2015

Accepted: 27 July 2015

Published: 27 August 2015

Author contributions: O.S., A.W., T.I., J.N., K.O., H.K., and T.Y. designed research; O.S., A.W., M.O., M.T., T.S., M.K., G.K., and H.M. performed research; O.S. analyzed data; O.S., A.W., M.T., and T.Y. wrote the paper.

Funding: the Ministry of Education, Culture, Sports and Technology of Japan: the Strategic Research Program for Brain Sciences. the Ministry of Education, Culture, Sports and Technology of Japan: the Mind/Brain Project. NIBB Collaborative Research Program: 13-308.

Conflict of Interest: The authors declare that there is no conflict of interest.

Corresponding author: Tetsuo Yamamori, Division of Brain Biology, National Institute for Basic Biology, 38 Myodaiji, Okazaki, Aichi 444-8585, Japan. E-mail: yamamori@nibb.ac.jp

Cite as: eNeuro 2015; 10.1523/ENEURO.0019-15.2015

Alerts: Sign up at eneuro.org/alerts to receive customized email alerts when the fully formatted version of this article is published.

Accepted manuscripts are peer-reviewed but have not been through the copyediting, formatting, or proofreading process.

This is an open-access article distributed under the terms of the Creative Commons Attribution 4.0 International (http://creativecommons.org/licenses/by/4.0), which permits unrestricted use, distribution and reproduction in any medium provided that the original work is properly attributed.

Copyright © 2015 Society for Neuroscience

eNeuro Accepted Manuscript

eNeuro Accepted Manuscript

eNeuro

http://eneuro.msubmit.net

eN-MNT-0019-15R1

In vivo two-photon imaging of dendritic spines in marmoset neocortex

This is a confidential document and must not be discussed with others, forwarded in any form, or posted on websites without the express written consent of eNeuro.

eNeuro Accepted Manuscript

1 **1. Manuscript title**

2 *In vivo* two-photon imaging of dendritic spines in marmoset neocortex

3 **2. Abbreviated title**

4 Two-photon imaging of spines in marmoset cortex

5 **3. Author names and affiliations**

6 Osamu Sadakane[1,2], Akiya Watakabe[1,2], Masanari Ohtsuka[1,2], Masafumi Takaji[1,2], Tetsuya
7 Sasaki[3], Masatoshi Kasai[4], Tadashi Isa[4], Go Kato[5], Junichi Nabekura[5], Hiroaki Mizukami[6],
8 Keiya Ozawa[6], Hiroshi Kawasaki[7], Tetsuo Yamamori[1,2]

9 [1]Laboratory for Molecular Analysis of Higher Brain Function, Brain Science Institute, RIKEN,
10 Wako, Saitama 351-0198, Japan, [2]Division of Brain Biology, National Institute for Basic
11 Biology, Aichi 444-8585, Japan, [3]Department of Ultrastructural Research, National Center of
12 Neurology and Psychiatry, National Institute of Neuroscience, Tokyo 187-8502, Japan, [4]Division
13 of Behavioral Development, National Institute for Physiological Science, Aichi 444-8585, Japan,
14 [5]Division of Homeostatic Development, National Institute for Physiological Science, Aichi 444-
15 8585, Japan, [6]Division of Genetic Therapeutics, Center for Molecular Medicine, Jichi Medical
16 University, Tochigi 329-0498, Japan, [7]Department of Biophysical Genetics, Graduate School of
17 Medical Sciences, Kanazawa University, Ishikawa 920-8640, Japan

18 **4. Author contributions**

19 O.S., A.W., T.I., J.N., K.O., H.K., and T.Y. designed research; O.S., A.W., M.O., M.T., T.S.,

eNeuro Accepted Manuscript

20 M.K., G.K., and H.M. performed research; O.S. analyzed data; O.S., A.W., M.T., and T.Y. wrote
21 the paper.

22 **5. Corresponding author**

23 Tetsuo Yamamori, Laboratory for Molecular Analysis of Higher Brain Function, Brain Science
24 Institute, RIKEN, Wako, Saitama 351-0198, Japan. E-mail: tetsuo.yamamori@riken.jp

25 **6. Number of figures**

26 6

27 **7. Number of tables**

28 1

29 **8. Number of multimedia**

30 0

31 **9. Number of words for abstract**

32 242

33 **10. Number of words for Significance Statement**

34 119

35 **11. Number of words for Introduction**

36 588

eNeuro Accepted Manuscript

37 **12. Number of words for Discussion**

38 790

39 **13. Acknowledgements**

40 The current affiliation of K.O. is as follows.

41 IMSUT Hospital, The Institute of Medical Science, The University of Tokyo, Tokyo, Japan.

42 Confocal images were acquired at Spectrography and Bioimaging Facility, NIBB Core Research

43 Facilities.

44 **14. Conflict of interest**

45 The authors declare that there is no conflict of interest.

46 **15. Funding sources**

47 This research is supported by the Strategic Research Program for Brain Sciences of the Ministry

48 of Education, Culture, Sports, Science and Technology, MEXT, Japan (to T.Y., T.I., and K.O.);

49 by the program for Brain Mapping by Integrated Neurotechnologies for Disease Studies

50 (Brain/MINDS) from Ministry of Education, Culture, Sports Science, MEXT, and the Japan

51 Agency for Medical Research and Development, AMED (to T.Y.); and by the NIBB

52 Collaborative Research Program (13-308)(to T.S.).

53

54

55

56

eNeuro Accepted Manuscript

57 **Abstract**

58 Two-photon microscopy in combination with a technique involving the artificial expression
59 of fluorescent protein has enabled the direct observation of dendritic spines in living brains.
60 However, the application of this method to primate brains has been hindered by the lack of
61 appropriate labeling techniques for visualizing dendritic spines. Here, we developed an AAV-
62 vector-based fluorescent protein expression system for visualizing dendritic spines *in vivo* in the
63 marmoset neocortex. For the clear visualization of each spine, the expression of reporter
64 fluorescent protein should be both sparse and strong. To fulfill these requirements, we amplified
65 fluorescent signals using the transactivator (tTA)-TET responsive element (TRE) system and by
66 titrating down the amount of Thy1S-promoter-driven tTA for sparse expression. By this method,
67 we were able to visualize dendritic spines in the marmoset cortex by two-photon microscopy *in*
68 *vivo* and analyze the turnover of spines in the prefrontal cortex. Our results demonstrated that
69 short spines in the marmoset cortex tend to change more frequently than long spines. The
70 comparison of *in vivo* samples with fixed samples showed that we did not detect all existing
71 spines by our method. Although we found glial cell proliferation, the damage of tissues caused
72 by window construction was relatively small judging from the comparison of spine length
73 between samples with or without window construction. Our new labeling technique for two-
74 photon imaging to visualize *in vivo* dendritic spines of the marmoset neocortex can be applicable
75 to examining circuit reorganization and synaptic plasticity in primates.

76 **Significance Statement**

77 Investigation of non-human primate brains is important for the understanding of the human
78 brain. However, because of technical difficulties, several important methods that have been used

eNeuro Accepted Manuscript

79 in rodent studies are not available for primate studies. Two-photon imaging of dendritic spines
80 has been used in rodent studies, which clarified the basis of neural circuit plasticity, but there has
81 been no report of the application of this imaging method to primate brains. Therefore, in this
82 study, we developed an AAV-vector-based fluorescent protein expression system for use in the
83 studies of the marmoset neocortex. Our approach enabled the sparse yet strong expression of
84 fluorescent protein in neurons. This labeling technique will be applicable to the research of
85 circuit reorganization of primate brains.

86 **Introduction**

87 Direct observation of fine neuronal morphologies such as dendritic spines in living brains
88 has been made possible with techniques involving the expression of fluorescent protein in
89 neurons of living animals in combination with two-photon microscopy. Many researchers prefer
90 to use transgenic mouse lines such as Thy1-GFP and Thy1-YFP mice for their imaging studies of
91 dendritic spines, because of the stable and strong expression of fluorescent protein in a
92 subpopulation of neurons in these lines (Feng et al., 2000; Grutzendler et al., 2002; Trachtenberg
93 et al., 2002; Holtmaat et al., 2005; Zuo et al., 2005; Kim and Nabekura, 2011; Fu et al., 2012).
94 The advancement of two-photon microscopy was also a key factor for the application of spine
95 imaging techniques to living animals (Denk et al., 1990; Denk and Svoboda, 1997). The long-
96 wavelength light used in two-photon microscopy penetrates a specimen with less scattering than
97 the short-wavelength light used in other conventional microscopies such as confocal microscopy;
98 thus, it is possible to observe signals from deep regions in a certain thick tissue.

99 Dendritic spine imaging by two-photon microscopy has almost been exclusively performed
100 on rodent brains, and there have been only a few studies in which the brains of larger species

eNeuro Accepted Manuscript

101 such as primates and carnivores have been examined. One major reason for the lack of studies of
102 such animals with larger brains is that there has been no standard method for *in vivo* imaging in
103 these species. Transgenic monkeys have been generated (Sasaki et al., 2009; Niu et al., 2010),
104 but no primate model that strongly expresses fluorescent protein for observing signals *in vivo* has
105 been established. Spine imaging of the primary visual cortex of ferrets using an expression
106 system with a virus vector was reported (Yu et al., 2011). In the case of primates, one group
107 studied the neuronal morphology in the primary visual cortex of macaque monkeys by *in vivo*
108 imaging using virus expression systems (Stettler et al., 2006; Yamahachi et al., 2009), but their
109 observation and analysis focused not on dendritic spines but on axonal structures. Using virus-
110 vector based methods for the labeling of neurons to study their morphology is difficult because
111 the high density of labeled neurons around the injection site makes the background signal
112 intensity also high, thus making such methods unsuitable for the observation of the morphology
113 of fine structures such as dendritic spines. Although dendritic spines in the primate cortex have
114 been extensively analyzed in fixed samples by dye injection methods (Elston et al., 1999; Oga et
115 al., 2013), there has been no report in which dendritic spines were imaged and analyzed *in vivo*
116 in primate brains.

117 In this report, we present a method of *in vivo* imaging of dendritic spines in the marmoset
118 neocortex. The marmoset was chosen as a model animal in our study because the flat surface of a
119 marmoset brain is advantageous for studying the entire cortical region. We had to overcome
120 mainly two technical problems in the *in vivo* visualization of dendritic spines in the marmoset
121 neocortex. We needed a stronger expression of fluorescent protein because the marmoset brain is
122 more opaque than the brains of smaller animals such as mice. In addition, we needed neurons to
123 be sparsely labeled, because the dense expression obtained by the virus vector method usually

eNeuro Accepted Manuscript

124 causes a high background signal intensity. We, therefore, used an AAV expression system for
125 the sparse and strong expression of the fluorescent protein in cortical neurons of marmosets, and
126 by two-photon microscopy we were able to observe more clearly dendritic spines labeled by
127 fluorescent proteins.

128 Materials and Methods

129 Animals

130 We used six marmosets (all males; body weight, 310–420 g; age, 13–22 months): five
131 animals for *in vivo* imaging and one animal for dye injection. All the protocols used in this study
132 were approved by the Institutional Animal Care and Use Committee of National Institutes of
133 Natural Sciences, Japan. The experiment was also conducted in accordance with the animal care
134 guidelines of the U.S. National Institutes of Health.

135 Plasmid construction and AAV preparation

136 The constructs used in this study are schematically shown in Figure 1A. The Thy1S
137 promoter was cloned from pThy1S-GFP for the sparse labeling of cortical neurons as previously
138 reported (Ako et al., 2011). Owing to capacity limitations of the AAV vector, we truncated
139 approximately 1.3 kb of the 5' region of the Thy1S promoter, which is reported to be non-
140 essential for the activity of the promoter (Vidal et al., 1990; Caroni, 1997). The plasmid
141 AAV:Thy1S-tTA was constructed by subcloning the DNA fragments containing the truncated
142 Thy1S promoter and tTA in pAAV-MCS (Agilent Technologies). The plasmid AAV:TRE-
143 hrGFP was constructed by replacing the tRFP sequence of AAV:TRE-tRFP (Watakabe et al.,
144 2014) with hrGFP.

145 AAV vectors used in this study have capsids of serotype 1. They were produced in HEK
146 293 cells using a helper-virus-free system and purified twice by $CsCl_2$ density gradient
147 centrifugation and titrated by Q-PCR as described previously (Konishi et al., 2008). The final
148 preparations obtained were dialyzed against PBS and diluted as described in the results section.
149 To prevent adhesion of the AAV vector to glass micropipettes, Pluronic-F68 (Sigma-Aldrich)
150 was added to the vector stock at 0.001%.

151 **Virus injection**

152 The marmosets were treated by intramuscular injections of ketamine (20 mg/kg; Daiichi
153 Sankyo) and xylazine (1 mg/kg; Bayer Health Care). Under deep anesthesia induced and
154 maintained by isoflurane (1–2%) inhalation (Abbott Laboratories), the head of the animal was
155 fixed to a stereotaxic apparatus. Pulse rate, SpO_2, and rectal temperature were continuously
156 monitored. A small hole was formed in the skull using a dental drill. To inject the viruses into the
157 cortex, the dura was punctured using the tip of a 27 G needle, through which a glass pipette was
158 slowly inserted to a depth of 500 µm from the cortical surface. Approximately 0.5 µl of a viral
159 solution was injected at a rate of 0.1 µl/min. For the imaging of the prefrontal cortex, our
160 injections were targeted at AP +18.5 mm, 2 mm to the right from the midline. Following the
161 viral injection, the hole was filled with Spongel, an absorbable gelatin sponge (Astellas Pharma
162 Inc.), and the scalp was sutured. Then the animal was returned to a cage and remained there until
163 the imaging sessions started. To prevent infection, ampicillin (40 mg/kg; Meiji Seika Pharma)
164 was administered intramuscularly. Carprofen (5 mg/kg; Pfizer) was administered intramuscularly
165 as an analgesic and an anti-inflammatory agent. Ampicillin and carprofen were administered
166 immediately after surgery and 2 subsequent days. We waited until an adequate level of gene

eNeuro Accepted Manuscript

eNeuro Accepted Manuscript

167 expression was obtained, which took at least 2 weeks.

168 ***In vivo* imaging**

169 Before an imaging session, we constructed an imaging window on the head of the animal.
170 The hole on the skull used for virus injection was expanded to a size of ~2 × 3 mm^2 using a
171 dental drill, and part of the dura above the injection site was deflected and resected ~1 mm in
172 diameter (Fig. 2A). A small coverglass of ~4 × 4 mm^2 size was fixed with dental cement on top
173 of the skull, and the space between the coverglass and the cortex was filled with an agarose gel
174 (1.5% in ACSF; type III-A, Sigma-Aldrich) to minimize vibration. A custom-made metal plate
175 with a hole of 11 mm inner diameter was glued to the skull (Figs. 2B and 2C). This plate was
176 used to fix the head of the animal during the imaging sessions. The same antibiotic, analgesic,
177 and anti-inflammatory agents as those used for the virus injections were administered
178 immediately after window construction and 2 subsequent days. We started the imaging sessions
179 from one to seven days after the imaging window construction (Fig. 2D).

180 *In vivo* two-photon imaging was performed using a FV1000MPE multiphoton laser
181 scanning microscope (Olympus) and a water immersion objective lens (25×; NA, 1.05;
182 Olympus). Two-photon excitation (920 nm) was provided by a mode-locked Ti:Sapphire laser
183 (MaiTai Deep See, Spectra-Physics). Fluorescence was detected using a multialkali
184 photomultiplier tube (PMT) without any filter in front of the PMT. The regions with
185 fluorescently labeled dendrites were identified without digital zoom (508 × 508 μm^2 field of
186 view). Then we used 8× digital zoom to acquire images of magnified sites including dendritic
187 spines at a resolution of 0.124 × 0.124 × 0.2 μm^3 (63 × 63 μm^2 field of view). These sites were
188 identified the following day and the images obtained on two consecutive days were analyzed.

189 Imaged sites were scattered around 508 × 508 μm^2 region and presumed to contain dendrites
190 originating from different neurons. During imaging sessions, the marmosets were anesthetized
191 with isoflurane (1–2%). Pulse rate, SpO_2, and rectal temperature were continuously monitored.

192 **Dye injection**

193 A marmoset was sedated with ketamine hydrochloride (25 mg/kg i.m.; Daiichi Sankyo) and
194 overdosed with sodium pentobarbital (75 mg/kg i.p.; Dainippon Sumitomo Pharma). The animal
195 was perfused intracardially with 0.1 M potassium phosphate-buffered saline (pH 7.2), followed
196 by 4% paraformaldehyde (Merck) in 0.1 M phosphate buffer (PB). A block of tissue was excised
197 from the PFC. Coronal slices of 250 µm thickness were prepared from the block. Slices were
198 incubated in 4,6-diamidino-2-phenylindole (DAPI; Sigma-Aldrich) solution to visualize the cell
199 bodies. Pyramidal cells were individually injected with 10 mM Alexa 568 (Alexa Fluor 568
200 Hydrazide in 200 mM KCl, A-10441, Thermo Fisher Scientific) under visual guidance with a
201 triple-band fluorescence filter (Semrock). The dye-injected neurons were imaged using a Leica
202 SP-8 confocal laser scanning microscope and a water immersion lens (63×; NA, 1.2; Leica) at a
203 resolution of 0.045 × 0.045 × 0.336 μm^3.

204 **Immunohistochemical analysis**

205 Marmosets were sedated with ketamine hydrochloride (25 mg/kg i.m.; Daiichi Sankyo) and
206 overdosed with sodium pentobarbital (75 mg/kg i.p.; Dainippon Sumitomo Pharma). The animals
207 were perfused transcardially with 0.9% NaCl and then fixed with 4% paraformaldehyde in 0.1 M
208 phosphate buffer (pH 7.4). Brain samples were cryoprotected with 30% sucrose/0.1 M phosphate
209 buffer (pH 7.0) and sectioned at thicknesses of 40–50 µm using a cryostat. For

eNeuro Accepted Manuscript

eNeuro Accepted Manuscript

210 immunofluorescence analysis, the sections were treated with 80% methanol/20% dimethyl
211 sulfoxide solution (Dent's solution) for more than 30 min, blocked with 10% fetal bovine serum,
212 2% bovine serum albumin, and 0.5% Triton X100 in TBS, pH 7.4, and then incubated overnight
213 with a primary antibody to hrGFP (1:4000; Vitality hrGFP rabbit polyclonal antibody; Agilent
214 Technologies Cat # 240141) at 4° C. After incubation with a Cy2-conjugated secondary antibody
215 (anti-rabbit Cy2, 1:1000; Jackson ImmunoResearch), the sections were counterstained with
216 Hoechst 33342 (1:2000; Molecular Probes). For immunostaining with anti-GFAP and Iba1
217 antibodies, rabbit polyclonal antibodies from Abcam (#AB7260) and Wako (#019-19741) were
218 used, respectively, as the primary antibodies, followed by staining with Cy3-conjugated anti-
219 rabbit IgG (1:1000; Jackson ImmunoResearch).

220 **Image analysis**

221 We used imageJ (US National Institutes of Health), Neurolucida (MBF Bioscience), and
222 custom-made software written on MATLAB (R2009a, MathWorks) for our image analysis.
223 Images were processed with a median filter (2.0 pixel radius) to reduce noise. Dendrites and
224 spines were traced and marked manually in a three-dimensional space. The loss or gain rate of
225 dendritic spines was calculated as the percentage of spines that appeared or disappeared on day 1,
226 relative to the total number of spines on day 0. The length of spines was measured from the tip of
227 the spine to the interface with the dendritic stalk (Ji et al., 2010).

228 **Statistical analysis**

229 All statistical analyses were performed using R (R Development Core Team, 2012). We
230 used the Wilcoxon rank sum test to compare between groups, and we corrected for multiple

eNeuro Accepted Manuscript

231 comparisons when required. Differences were considered to be significant when $p < 0.05$.
232 Measurements are reported as mean and SD. The values of statistical power were calculated
233 using G*Power (http://www.gpower.hhu.de/en.html) and presented in Table 1. Experimental
234 animals were randomly assigned to *in vivo* or *ex vivo* conditions.

235 **Results**

236 **Sparse and strong expression system for spine visualization**

237 To observe the dendritic spines of neurons in the marmoset cortex *in vivo*, there are two
238 requirements: strong and sparse expression of fluorescent protein. The scattering of light in
239 living tissues prevents weak signals from being captured by the detector, particularly in the
240 marmoset brain, which is more opaque than the mouse brain; thus, a strong expression is
241 required. Moreover, to observe fine structures such as spines, the expression of fluorescent
242 protein should be sufficiently strong to adequately label these fine structures. Sparse expression
243 is also required to reduce the intensity of background signals. Even when the expression level of
244 fluorescent protein in each neuron is sufficiently strong, a dense expression of fluorescent protein
245 in neighboring neuronal structures such as dendrites and axons makes the intensity of
246 background signals high, thus preventing the clear observation of dendritic spines.
247 Our strategy to achieve the requirements described above was to combine the transactivator
248 (tTA)-TET responsive element (TRE) system and Thy1S promoter (Ako et al., 2011) using two
249 virus vectors. We constructed two AAV vectors: one had the tTA component under the control
250 of the Thy1S promoter (AAV:Thy1S-tTA) and the other had hrGFP under the control of TRE
251 (AAV:TRE-hrGFP). Figure 1A shows a schematic drawing of our virus constructs. Ako et al.
252 (2011) developed the Thy1S promoter to sparsely label the fine structures of neurons in the

eNeuro Accepted Manuscript

253 mouse neocortex. When expressed by electroporation in the mouse neocortex, the Thy1S
254 promoter drives the gene expression only in a small number of pyramidal neurons in layers 2/3
255 and 5. In our expression system, the tTA-TRE system was driven only in Thy1S-positive cells.
256 Hioki et al. (2009) showed that the tTA-TRE system is effective in amplifying transgene
257 expression. The tTA-TRE system has two components, one is tTA and the other is TRE. When
258 tTA binds to the TRE component, the transcription of hrGFP that is under the control of the TRE
259 component is strongly activated.

260 We injected a mixture of these virus vectors into the marmoset neocortex and first examined
261 the expression in fixed brain samples (Fig. 1B). We were interested in the density of hrGFP-
262 positive neurons and the visibility of each dendrite. In our preliminary mouse experiment, we
263 found that maintaining the concentration of AAV:TRE-hrGFP at 4.6×10^{12} vector genomes
264 (vg)/ml and reducing the concentration of AAV:Thy1PS-tTA to approximately 1/500 of the TRE
265 vector (8.8×10^{9} vg/ml) leads to the sparse but strong expression of the fluorescent protein (data
266 not shown). On the basis of this finding, we tested various concentrations of AAV:Thy1S-tTA
267 relative to that of AAV:TRE-hrGFP in marmosets. At an AAV:Thy1S-tTA to AAV:TRE-hrGFP
268 concentration ratio of 1:200, the number of hrGFP-positive neurons was relatively high (Fig. 1B,
269 left). At a concentration ratio of 1:2000, the number of hrGFP-positive neurons was too small
270 (Fig. 1B, right). An AAV:Thy1S-tTA to AAV:TRE-hrGFP concentration ratio of 1:500 yielded
271 the most desirable signals in terms of intensity and density (Fig. 1B, middle).

272 We emphasize the importance of amplifying the expression level of hrGFP using the tTA-
273 TRE system. Simply reducing the titer of the virus leads to a low expression level, thus making it
274 difficult to observe spines *in vivo*. The combination of titration and amplification was required
275 for the clear visualization of dendritic spines in the marmoset neocortex.

eNeuro Accepted Manuscript

276 ***In vivo* visualization of dendritic spines in neocortex**

277 To test the feasibility of our viral expression system *in vivo*, we injected the virus into the
278 marmoset neocortex. After two weeks of expression period, we acquired images from living
279 animals under anesthesia induced by isoflurane. Figure 3 shows *in vivo* captured images. We
280 were able to visualize each dendritic spine using our virus constructs (Figs. 3C–E). We observed
281 the dendritic spines of apical dendrites located in layer 1. We were also able to observe the cell
282 bodies located at a depth of approximately 300 μm from the pia (Fig. 3F at 220 μm and Fig. 3G
283 at 330 μm).

284 We then acquired images repeatedly from the same region over time. Figure 4 shows time-
285 lapse images of the dorsolateral prefrontal cortex, presumably area 8B or 9. The images of the
286 same region of the dendrites were taken over time at 24 hour intervals. During these imaging
287 sessions, the clarity of the imaging window was maintained. Because our samples contained a
288 relatively small number of hrGFP-positive neurons per injected site, we were able to easily
289 identify the same dendrite that we observed in the previous imaging session. The overall shapes
290 of dendrites did not change over this imaging period (Fig. 4A, top and bottom). We marked each
291 spine on the two images (Day 0 and Day 1) by comparing these images side by side, and
292 identified the spines that were "gained" or "lost" during this time interval (Fig. 4B and C). In our
293 experiments, we analyzed 779 spines (12 sites, 34 dendrites, 3 animals, total dendrite length of
294 2238 μm); of these spines, 51 were gained (mean across sites, 6.4%; SD, 4.2) and 49 were lost
295 (mean across sites; 5.6%, SD, 3.6) (Fig. 4D). The loss or gain rate at 1 day interval observed in
296 this study was similar to those in previous studies of layer 5 neurons of the somatosensory cortex
297 of transgenic mice (~12% in 3 days for both loss and gain; Kim and Nabekura, 2011) and layer
298 2/3 neurons of ferret V1 by the virus vector method (~4% in 1 day for both loss and gain; Yu et

eNeuro Accepted Manuscript

299 al., 2011). We measured spine length by manual tracing using Neurolucida software, and
300 examined the difference between the distribution of the spines that persisted and that of the
301 spines that changed (gained and lost) over the period of imaging. We observed the tendency that
302 the changed spines were shorter than those that persisted (Wilcoxon rank sum test, changed vs
303 persisted, p = 0.0009[a]), which means that shorter spines tend to be gained or lost (Fig. 4E).
304 One of the concerns raised in the two-photon imaging of dendritic spines in mice studies
305 was the activation of glial cells under invasive procedures. Because our methods in the marmoset
306 neocortex include invasive procedures of virus injection and dura opening, we checked the
307 activation of glial cells in our sample of the prefrontal cortex that was used for the *in vivo*
308 imaging study. We observed the activation of both astrocytes (GFAP, Figs. 5A–C) and
309 microglias (Iba1, Figs. 5D–F) around the injection site. This observation indicated that
310 experimenters should carefully choose the experimental paradigm when applying the method
311 presented in this paper (see Discussion).

312 **Comparison between *in vivo* and fixed samples**

313 To evaluate our *in vivo* two-photon microscope images of dendritic spines in the marmoset
314 neocortex, we compared them with those of fixed samples. We wanted to determine whether we
315 observed all existing spines or only a subpopulation of these spines. To clarify this point, we
316 used the method which was employed to identify the morphological differences of basal
317 dendrites of pyramidal neurons in different cortical areas from various species including
318 marmosets and macaques (Elston et al., 1999; Oga et al., 2013). We injected the dye Alexa 568
319 into the neurons in the coronal sections of the marmoset prefrontal cortex, corresponding to the
320 region we imaged under *in vivo* condition, and observed the spines of apical dendrites of these

eNeuro Accepted Manuscript

321 dye-injected neurons under a confocal microscope (Fig. 6A; one animal, 15 sites, 22 dendrites,
322 1219 spines, total dendrite length of 1125 μm). Our injection well labeled dendritic spines in the
323 distal region of apical dendrites. We quantified the density and shape of spines in our fixed
324 samples by manual tracing using Neurolucida software, and we compared the results with our *in*
325 *vivo* data. The density of spines under our *in vivo* condition (mean, 0.36 spines/μm; SD, 0.14)
326 was significantly lower than that in dye-stained samples (mean, 1.12 spines/μm; SD, 0.21)
327 (Wilcoxon rank sum test with Holm correction, p = 0.00038[b]; Fig. 6B). The spines observed by
328 *in vivo* two-photon imaging were shorter than those in dye-stained fixed tissues (Wilcoxon rank
329 sum test with Holm correction, $p = 7.6 \times 10^{-12}$ [c]; Fig. 6C). This comparison of results between *in*
330 *vivo* two-photon imaging and dye staining of fixed samples indicated that the observation of
331 dendritic spines by the *in vivo* imaging system still has certain limitations.
332 As for the causes of these limitations, there are two possibilities. The most likely possibility
333 is that because of inefficient visualization, we underestimated the number of spines in *in vivo*
334 imaging. The second possibility is that the damage caused by AAV injection decreased the
335 number of spines. To determine which of these two possibilities is true, we
336 immunohistochemically stained our samples used *in vivo* imaging with the antibody to hrGFP
337 (IHC samples), and then observed these fixed samples by confocal microscopy (two animals, 15
338 sites, 20 dendrites, 839 spines, total dendrite length of 951 μm). Although one may consider the
339 comparison between the observation *in vivo* and the same dendritic segments identified in fixed
340 condition, it was practically difficult for us to identify the same dendritic segments in the more
341 crowded fixed samples because immunohistochemical staining amplified the signals even in
342 dendrites that express hrGFP weakly. Thus, here we compared the observation *in vivo* with the
343 dendritic segments at the matching regions from the same samples. The spine density of IHC

eNeuro Accepted Manuscript

344 samples was much higher than that of samples in *in vivo* imaging (Wilcoxon rank sum test with
345 Holm correction, $p = 0.00038^{d}$; Fig. 6B), suggesting that we were not able to detect weaker
346 signals under *in vivo* two-photon imaging. However, the spine density of IHC samples was lower
347 than that of dye-stained fixed samples (Wilcoxon rank sum test with Holm correction, $p =$
348 0.0028^{e}), which also suggests that there may have been some losses of spines owing to tissue
349 damage, as mentioned above. However, the distribution of spine length of IHC samples largely
350 overlapped with that of dye-stained fixed samples but not with that of *in vivo* samples (Fig. 6C).
351 This indicates that the window construction only mildly affected dendritic spines (Wilcoxon rank
352 sum test with Holm correction; IHC vs Dye, $p = 0.64^{f}$; IHC vs *in vivo*, $p = 2.2 \times 10^{-10\ g}$).

353 **Discussion**

354 In this study, we established a method of visualizing dendritic spines in the marmoset cortex
355 by *in vivo* two-photon imaging using a virus expression system. To the best of our knowledge,
356 this is the first demonstration of two-photon imaging of dendritic spines in the neocortex of a
357 living primate.

358 **Merits of this method**

359 By virus injection, we can control gene expression and monitor the morphology of
360 transduced neurons without affecting other parts of the brain. Even though transgenic marmoset
361 lines in which a specific neuronal population expresses fluorescent protein may be available for
362 *in vivo* imaging in the near future, virus expression systems have their own merits. One
363 advantage is the shorter time required for their preparation. Generating transgenic primate lines
364 requires a much longer time. Another merit is region-specific manipulation. The use of the

eNeuro Accepted Manuscript

365 combination of transgenic animals and virus expression systems will be beneficial in future
366 studies. For example, a specific cell type can be targeted by the transgenic insertion of an
367 appropriate promoter, and the local expression of a gene may be induced by an appropriate virus
368 expression system.

369 **Technical considerations**

370 Our method presented in this paper still has some limitations. First, there may have been
371 tissue damage due to our procedures in our study. The dura of the marmoset brain is more
372 opaque than that of the mouse brain, so we dissected the dura to observe dendritic spines *in vivo*
373 by two-photon imaging. This procedure may be more invasive than that used in mice. In mice,
374 some researchers argued that even removing the skull could perturb the underlying brain tissues
375 and make dendritic spines more unstable (Xu et al., 2007). Indeed as shown in Figure 5, we
376 observed the activation of glial cells around the injection site. Since a previous study in the
377 primary visual cortex of the ferret (Yu et al., 2011) was conducted in a comparable condition like
378 ours (using the Sindbis virus), and examined the activity dependent morphological plasticity of
379 dendritic spines by comparing active and inactive ocular dominance column, likewise our
380 methods presented in this paper may be applicable to studies which compare morphological
381 plasticity in different conditions, such as the level of sensory input or the state of learning.
382 Therefore, we believe that our method is an important technical improvement towards the
383 understanding of function of the primate neocortex. However, we have to further improve our
384 methods so that the tissue could be less damaged. One possible improvement is to construct an
385 imaging window which permits the longer imaging period, and allows waiting for time until the
386 activity of glial cells subsides. Another improvement could be developing procedures to acquire

eNeuro Accepted Manuscript

387 images through the dura. In the process of developing the methods described in this paper, we
388 are on the way to acquire images of axons through the intact dura of the marmoset cortex. In
389 future studies, the improvement of the method for imaging dendritic spines through the dura will
390 lead to a less invasive imaging.

391 Second limitation is in detecting weak signals as shown in Figure 6. Therefore, we need to
392 amplify such signal, or to use a detector with high sensitivity.

393 **Importance of examining spines in brains of living primates**

394 The majority of imaging studies of spines were carried out on mice, because many
395 molecular biological techniques are available for mice. Although experiments using mice are
396 important, there are certain functions and structures that only primates have acquired during the
397 course of their evolution. For example, the area specialization of the neocortex is far more
398 evolved in primates than in rodents. In previous studies, the area-specific gene expression
399 profiles in the primate neocortex were examined (Yamamori and Rockland, 2006; Yamamori,
400 2011; Bernard et al., 2012). Genes selectively expressed in association areas (Komatsu et al.,
401 2005; Takaji et al., 2009; Sasaki et al., 2010) and the primary visual cortex (Takahata et al.,
402 2006; Watakabe et al., 2009) were reported. Importantly, area-selective expressions of these
403 genes are not observed in rodents (Yamamori, 2011). In relation to the gene expression patterns
404 in different cortical areas, previous studies have shown that the density of spines significantly
405 differs among different areas of the primate neocortex (Elston et al., 1999, 2005; Elston and
406 Rockland, 2002). There is a smaller difference in the density of spines among different cortical
407 areas in mice than in primates (Ballesteros-Yáñez et al., 2006). In addition, previous studies by
408 *in vivo* two-photon imaging of spines in mice showed that there is no significant difference in

eNeuro Accepted Manuscript

409 morphological plasticity among different areas (Zuo et al., 2005). It is, therefore, of great interest
410 to us to determine whether there is a difference in morphological plasticity among different areas
411 in the primate brain, which we are going to investigate using the method described in this report.

412 **References**

413 Ako R, Wakimoto M, Ebisu H, Tanno K, Hira R, Kasai H, Matsuzaki M, Kawasaki H (2011)
414 Simultaneous visualization of multiple neuronal properties with single-cell resolution in the
415 living rodent brain. Mol Cell Neurosci 48:246–257.

416 Ballesteros-Yáñez I, Benavides-Piccione R, Elston GN, Yuste R, DeFelipe J (2006) Density and
417 morphology of dendritic spines in mouse neocortex. Neuroscience 138:403–409.

418 Bernard A et al. (2012) Transcriptional architecture of the primate neocortex. Neuron 73:1083–
419 1099.

420 Caroni P (1997) Overexpression of growth-associated proteins in the neurons of adult transgenic
421 mice. J Neurosci Methods 71:3–9.

422 Denk W, Strickler JH, Webb WW (1990) Two-photon laser scanning fluorescence microscopy.
423 Science 248:73–76.

424 Denk W, Svoboda K (1997) Photon upmanship: Why multiphoton imaging is more than a
425 gimmick. Neuron 18:351–357.

426 Elston GN, Benavides-Piccione R, DeFelipe J (2005) A study of pyramidal cell structure in the
427 cingulate cortex of the macaque monkey with comparative notes on inferotemporal and
428 primary visual cortex. Cereb Cortex 15:64–73.

429 Elston GN, Rockland KS (2002) The pyramidal cell of the sensorimotor cortex of the macaque
430 monkey: phenotypic variation. Cereb Cortex 12:1071–1078.

431 Elston GN, Tweedale R, Rosa MGP (1999) Cellular heterogeneity in cerebral cortex: A study of
432 the morphology of pyramidal neurones in visual areas of the marmoset monkey. J Comp
433 Neurol 415:33–51.

434 Feng G, Mellor RH, Bernstein M, Keller-Peck C, Nguyen QT, Wallace M, Nerbonne JM,
435 Lichtman JW, Sanes JR (2000) Imaging neuronal subsets in transgenic mice expressing
436 multiple spectral variants of GFP. Neuron 28:41–51.

eNeuro Accepted Manuscript

437 Fu M, Yu X, Lu J, Zuo Y (2012) Repetitive motor learning induces coordinated formation of
438 clustered dendritic spines in vivo. Nature 483:92–95.

439 Grutzendler J, Kasthuri N, Gan W-B (2002) Long-term dendritic spine stability in the adult
440 cortex. Nature 420:812–816.

441 Hioki H, Kuramoto E, Konno M, Kameda H, Takahashi Y, Nakano T, Nakamura KC, Kaneko T
442 (2009) High-level transgene expression in neurons by lentivirus with Tet-Off system.
443 Neurosci Res 63:149–154.

444 Holtmaat AJ, Trachtenberg JT, Wilbrecht L, Shepherd GM, Zhang X, Knott GW, Svoboda K
445 (2005) Transient and persistent dendritic spines in the neocortex in vivo. Neuron 45:279–
446 291.

447 Ji Y, Lu Y, Yang F, Shen W, Tang TT-T, Feng L, Duan S, Lu B (2010) Acute and gradual
448 increases in BDNF concentration elicit distinct signaling and functions in neurons. Nat
449 Neurosci 13:302–309.

450 Kim SK, Nabekura J (2011) Rapid synaptic remodeling in the adult somatosensory cortex
451 following peripheral nerve injury and its association with neuropathic pain. J Neurosci
452 31:5477–5482.

453 Komatsu Y, Watakabe A, Hashikawa T, Tochitani S, Yamamori T (2005) Retinol-binding
454 protein gene is highly expressed in higher-order association areas of the primate neocortex.
455 Cereb Cortex 15:96–108.

456 Konishi M, Kawamoto K, Izumikawa M, Kuriyama H, Yamashita T (2008) Gene transfer into
457 guinea pig cochlea using adeno-associated virus vectors. J Gene Med 10:610–618.

458 Niu Y et al. (2010) Transgenic rhesus monkeys produced by gene transfer into early-cleavage-
459 stage embryos using a simian immunodeficiency virus-based vector. Proc Natl Acad Sci U
460 S A 107:17663–17667.

461 Oga T, Aoi H, Sasaki T, Fujita I, Ichinohe N (2013) Postnatal development of layer III pyramidal
462 cells in the primary visual, inferior temporal, and prefrontal cortices of the marmoset. Front
463 Neural Circuits 7:31.

464 R Development Core Team (2012) R: A language and environment for statistical computing. R
465 Foundation for Statistical Computing.

466 Sasaki E et al. (2009) Generation of transgenic non-human primates with germline transmission.
467 Nature 459:523–527.

468 Sasaki T, Komatsu Y, Watakabe A, Sawada K, Yamamori T (2010) Prefrontal-enriched SLIT1
469 expression in old world monkey cortex established during the postnatal development. Cereb

eNeuro Accepted Manuscript

470 Cortex 20:2496–2510.

471 Stettler DD, Yamahachi H, Li W, Denk W, Gilbert CD (2006) Axons and synaptic boutons are
472 highly dynamic in adult visual cortex. Neuron 49:877–887.

473 Takahata T, Komatsu Y, Watakabe A, Hashikawa T, Tochitani S, Yamamori T (2006) Activity-
474 dependent expression of occ1 in excitatory neurons is a characteristic feature of the primate
475 visual cortex. Cereb Cortex 16:929–940.

476 Takaji M, Komatsu Y, Watakabe A, Hashikawa T, Yamamori T (2009) Paraneoplastic antigen-
477 like 5 gene (PNMA5) is preferentially expressed in the association areas in a primate
478 specific manner. Cereb Cortex 19:2865–2879.

479 Trachtenberg JT, Chen BE, Knott GW, Feng G, Sanes JR, Welker E, Svoboda K (2002) Long-
480 term in vivo imaging of experience-dependent synaptic plasticity in adult cortex. Nature
481 420:788–794.

482 Vidal M, Morris R, Grosveld F, Spanopoulou E (1990) Tissue-specific control elements of the
483 Thy-1 gene. EMBO J 9:833–840.

484 Watakabe A, Komatsu Y, Sadakane O, Shimegi S, Takahata T, Higo N, Tochitani S, Hashikawa
485 T, Naito T, Osaki H, Sakamoto H, Okamoto M, Ishikawa A, Hara SI, Akasaki T, Sato H,
486 Yamamori T (2009) Enriched expression of serotonin 1B and 2A receptor genes in macaque
487 visual cortex and their bidirectional modulatory effects on neuronal responses. Cereb Cortex
488 19:1915–1928.

489 Watakabe A, Takaji M, Kato S, Kobayashi K, Mizukami H, Ozawa K, Ohsawa S, Matsui R,
490 Watanabe D, Yamamori T (2014) Simultaneous visualization of extrinsic and intrinsic axon
491 collaterals in Golgi-like detail for mouse corticothalamic and corticocortical cells: a double
492 viral infection method. Front Neural Circuits 8:110.

493 Xu HT, Pan F, Yang G, Gan WB (2007) Choice of cranial window type for in vivo imaging
494 affects dendritic spine turnover in the cortex. Nat Neurosci 10:549–551.

495 Yamahachi H, Marik SA, McManus JNJ, Denk W, Gilbert CD (2009) Rapid axonal sprouting
496 and pruning accompany functional reorganization in primary visual cortex. Neuron 64:719–
497 729.

498 Yamamori T (2011) Selective gene expression in regions of primate neocortex: Implications for
499 cortical specialization. Prog Neurobiol 94:201–222.

500 Yamamori T, Rockland KS (2006) Neocortical areas, layers, connections, and gene expression.
501 Neurosci Res 55:11–27.

502 Yu H, Majewska AK, Sur M (2011) Rapid experience-dependent plasticity of synapse function

503 and structure in ferret visual cortex in vivo. Proc Natl Acad Sci 108:21235–21240.

504 Zuo Y, Lin A, Chang P, Gan WB (2005) Development of long-term dendritic spine stability in
505 diverse regions of cerebral cortex. Neuron 46:181–189.

506

507 **Figure Legends**

508 **Figure 1. Thy1S promoter drives sparse expression of hrGFP in marmoset cortex**

509 *A*, Schematic illustration of virus constructs. *B*, The expression of hrGFP at different
510 concentrations of virus injection was imaged in fixed brain samples using two-photon
511 microscopy. Left, low concentration; middle, medium concentration; right, high concentration.
512 Note the difference in labeled cell density at different concentrations. Maximum intensity
513 projections of 71, 71, and 51 slices for left, middle, and right panels, respectively at intervals of 5
514 µm. Scale bar, 100 µm.

515 **Figure 2. Construction of imaging window**

516 *A*, Craniotomy and durotomy over the target region around the somatosensory cortex. The
517 exposed target region of the marmoset cortex is shown. Scale bar, 500 µm. *B*, Illustration of
518 metal plate used in this study. *C*, Picture showing the metal plate for fixation, attached to the
519 marmoset head. Scale bar, 10 mm. *D*, Experimental schedule.

520 **Figure 3. Dendritic spines imaged by *in vivo* two-photon microscopy**

521 *A*, Maximum intensity projection of the images acquired *in vivo* two-photon imaging of
522 marmoset cortex. *B*, Side view of three-dimensional reconstruction of the images of the same site
523 shown in A. The depths of the areas shown in F and G are indicated by dashed lines. *C*, Image
524 plane near pial surface. *D*, Magnified image of boxed area in C. *E*, Magnified image of boxed

eNeuro Accepted Manuscript

525 area in D showing dendritic spines. *F*, Image plane at depth of 220 µm showing soma and basal
526 dendrites. *G*, Image plane at depth of 330 µm. (Scale bars: A and B, 100 µm; C, 50 µm; D, 5 µm;
527 E, 2 µm; F and G, 50 µm.)

528 **Figure 4. Time-lapse imaging of spines in prefrontal cortex**
529 *A*, The same dendritic regions in the prefrontal cortex were imaged at 24 hour intervals. The top
530 panel shows an image acquired on day 0 (7 days after craniotomy) and the bottom panel shows
531 an image acquired on day 1. Scale bar, 5 µm. *B*, The gained spines were identified by manual
532 inspection of two images acquired at 24 hour intervals. A filled rectangle indicates the position
533 of an example of a gained spine. Scale bar, 1µm. *C*, The same as B for lost spines. Filled
534 triangles indicate the positions of lost spines. *D*, Box plots showing spine turnover rate. The open
535 circles in box plots indicate mean values. Black dots indicate values for each site. The whiskers
536 extend to the largest and smallest values within 1.5 times the interquartile range. *E*, Cumulative
537 distributions of spine length in persisting, gained, and lost populations.

538 **Figure 5. Activation of glial cells**
539 *A*, Confocal image of a sample immunohistochemically stained with anti-GFAP antibody. Scale
540 bar, 500 µm. *B*, Magnified image of left boxed area in A, near injection site. *C*, Magnified image
541 of right boxed area in A, distal region from injection site. Scale bar, 200 µm. *D*, Confocal image
542 of sample immunohistochemically stained with anti-Iba1 antibody. Scale bar, 500 µm. *E*,
543 Magnified image of left boxed area in C, near injection site. *F*, Magnified image of right boxed
544 area in C, distal region from injection site. Scale bar, 200 µm.

eNeuro Accepted Manuscript

eNeuro Accepted Manuscript

545 **Figure 6. Comparison of dendritic spines between *in vivo* and *ex vivo* observations**

546 *A*, Confocal images of *ex vivo* dye-injected samples. Scale bars: top, 100 µm; bottom, 5 µm. *B*,
547 Box plots showing spine densities in *in vivo* and *ex vivo* populations. The open circles in box
548 plots indicate mean values. Black dots indicate values for each site. The whiskers extend to the
549 largest and smallest values within 1.5 times the interquartile range. *C*, Spine densities of *in vivo*,
550 dye-injected, and IHC samples. *D*, Cumulative distribution of spine length under *in vivo* and *ex*
551 *vivo* conditions.

552 **Table**

553 **Table 1. Statistical table**

	Data structure	Type of test	Power
a	Normality not assumed	Wilcoxon rank sum test	0.51
b	Normality not assumed	Wilcoxon rank sum test with Holm correction	1.00
c	Normality not assumed	Wilcoxon rank sum test with Holm correction	0.97
d	Normality not assumed	Wilcoxon rank sum test with Holm correction	1.00

e	Normality not assumed	Wilcoxon rank sum test with Holm correction	0.79
f	Normality not assumed	Wilcoxon rank sum test with Holm correction	0.51
g	Normality not assumed	Wilcoxon rank sum test with Holm correction	1.00

554

eNeuro Accepted Manuscript

eNeuro Accepted Manuscript

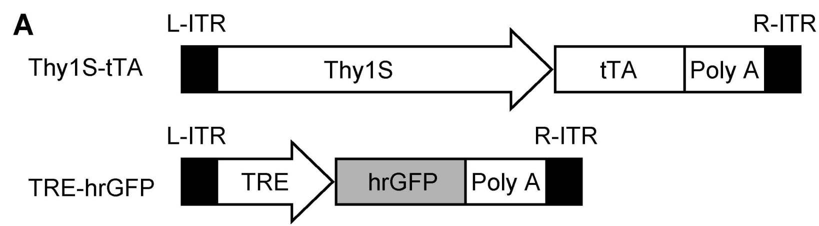

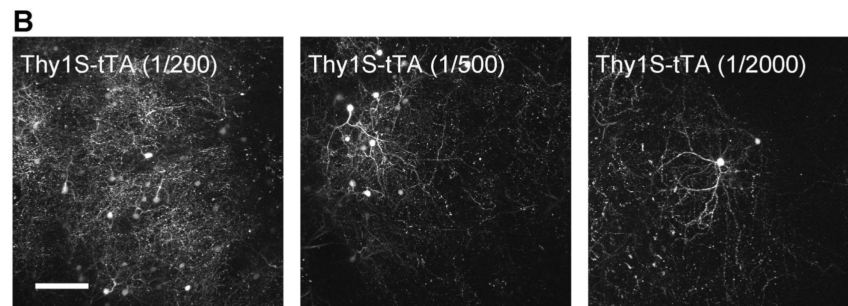

eNeuro Accepted Manuscript

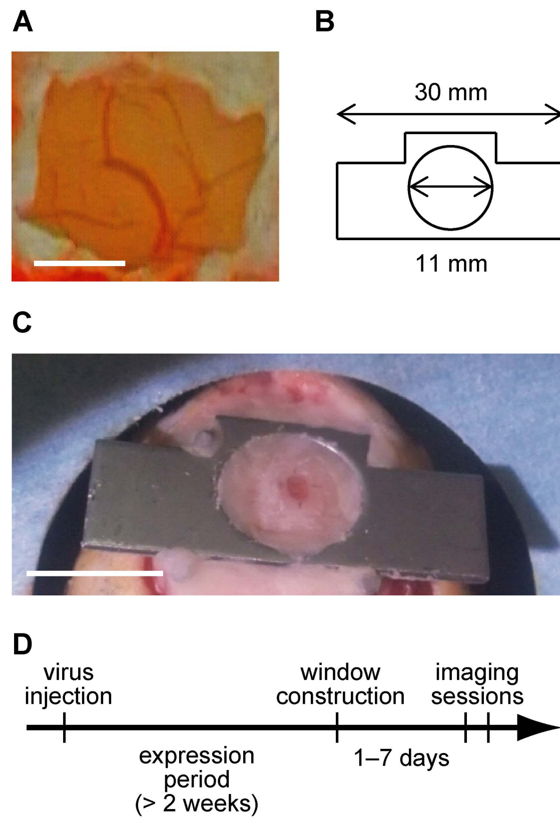

eNeuro Accepted Manuscript

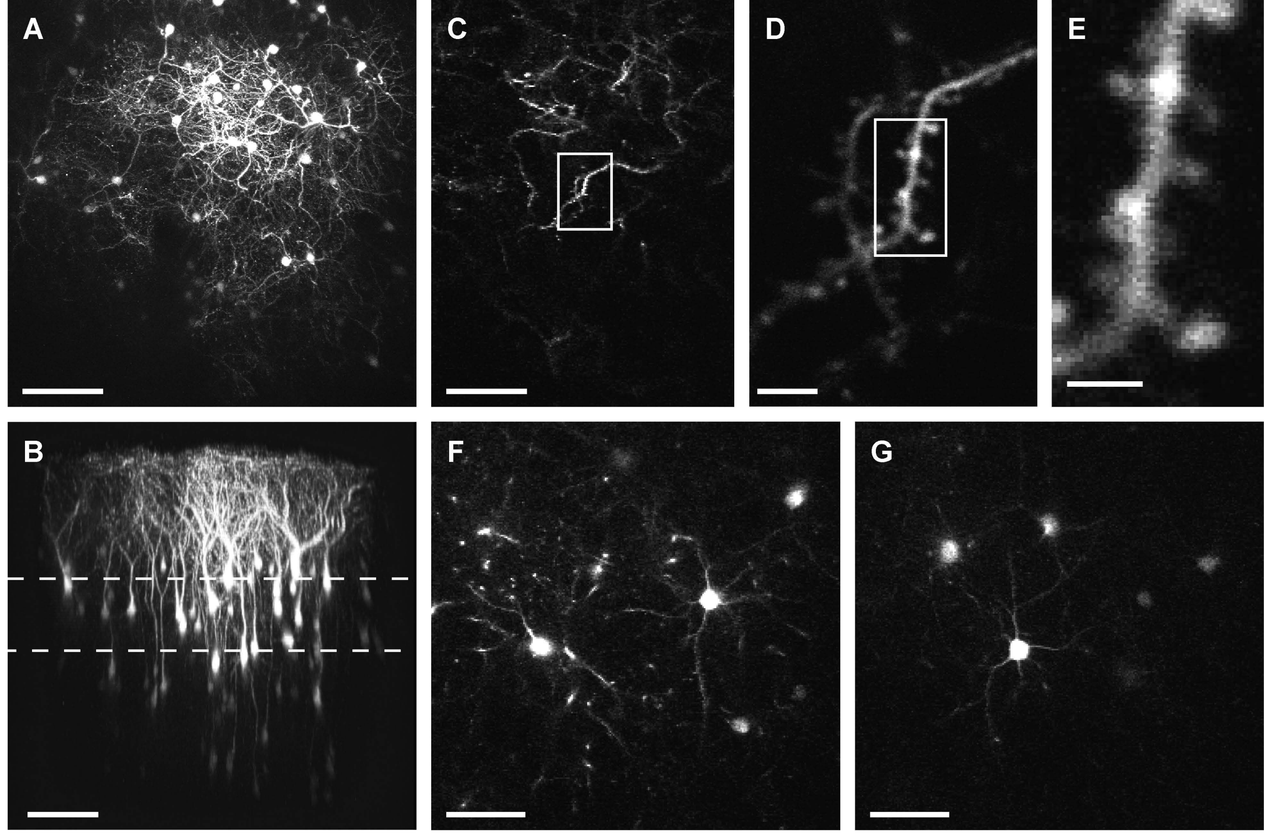

eNeuro Accepted Manuscript

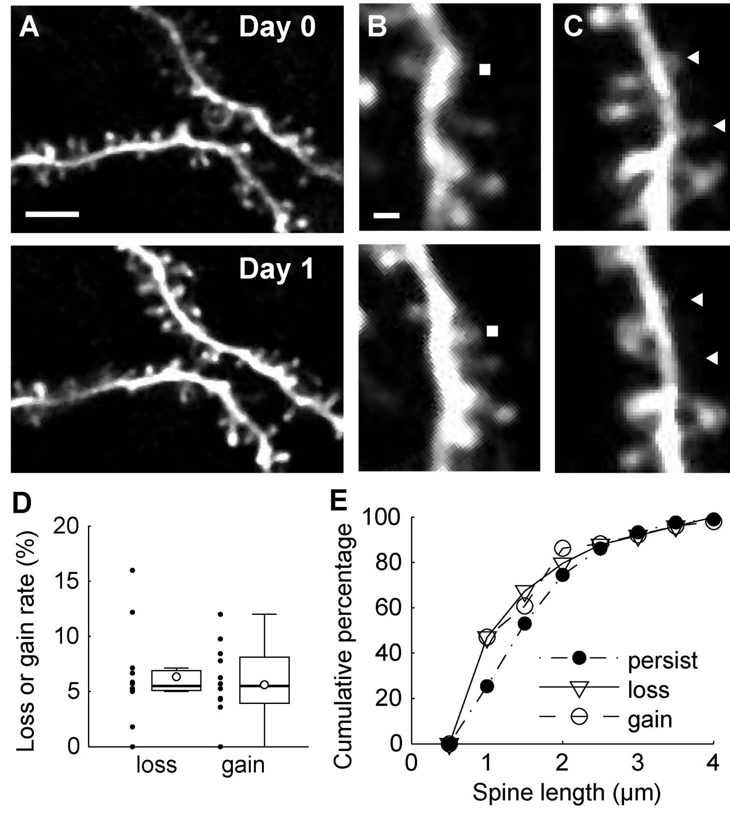

eNeuro Accepted Manuscript

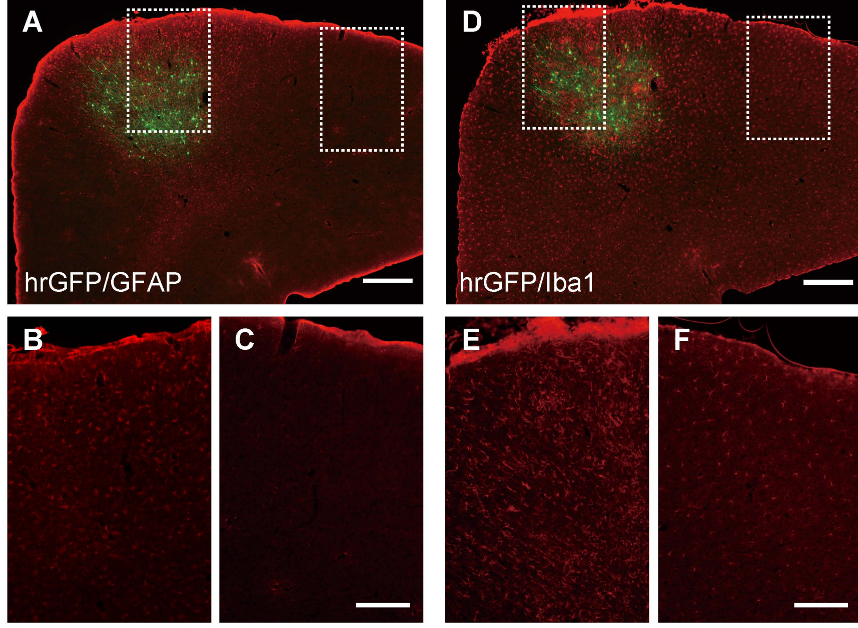

eNeuro Accepted Manuscript